Applied Catalysis B: Environmental 178 (2015) 74–81

Contents lists available at ScienceDirect

Applied Catalysis B: Environmental

journal homepage: www.elsevier.com/locate/apcatb

Boron doped TiO_2 catalysts for photocatalytic ozonation of aqueous mixtures of common pesticides: Diuron, o-phenylphenol, MCPA and terbuthylazine

D.H. Quiñones [a], A. Rey [a,*], P.M. Álvarez [a], F.J. Beltrán [a], G. Li Puma [b]

[a] Dpto. Ingeniería Química y Química Física, Universidad de Extremadura, Avda. Elvas s/n, 06006 Badajoz, Spain
[b] Environmental Nanocatalysis and Photoreaction Engineering, Department of Chemical Engineering, Loughborough University, LE11 3TU Loughborough, United Kingdom

ARTICLE INFO

Article history:
Received 11 July 2014
Received in revised form 10 October 2014
Accepted 12 October 2014
Available online 18 October 2014

Keywords:
Photocatalytic ozonation
Boron doped TiO_2
Boron leaching
Pesticides
Solar light

ABSTRACT

TiO_2 and B-doped TiO_2 catalysts were synthesized using a sol–gel procedure. The photocatalysts were characterized by ICP-EOS, N_2 adsorption–desorption, XRD, XPS, and DR-UV-Vis spectroscopy. Four recalcitrant pesticides (diuron, o-phenylphenol, 2-methyl-4-chlorophenoxyacetic acid (MCPA) and terbuthylazine) were subjected to degradation by ozonation, photolytic ozonation, photocatalysis and photocatalytic ozonation using the prepared catalysts under simulated solar irradiation in a laboratory scale system. The B-doped TiO_2 catalysts, with 0.5–0.8 wt.% of interstitial boron, were more active than bare TiO_2 for the removal and mineralization of the target compounds. The combination of ozonation and photocatalysis led to faster mineralization rates than the treatment methods considered individually and allowed the complete removal of the pesticides below the regulatory standards. The B-doped catalyst was stable and maintained 75% mineralization after three consecutive runs.

1. Introduction

Water pollution and scarcity is a global concern. Agriculture is the industrial activity that has the major impact on aquatic ecosystems, due to the large volumes of water consumed (70% of the world accessible freshwater [1]) and the high content of organic substances (pesticides and fertilizers) which are dispersed in aqueous environments by runoff or leaching. Many pollutants found in water ecosystems are recalcitrant to some degree to biological and physicochemical processes that are conventionally used in wastewater treatment plants. In the last decades, Advanced Oxidation Processes (AOPs) have being pointed out as effective alternatives to deal with this kind of contaminants. These technologies can generate non-selective, highly reactive and short-life oxidizing species, which in turn can completely degrade organic pollutants through oxidation reactions [2].

Photocatalysis is one of the most successfully and extensively studied AOP. It involves the excitation of a semiconductor through the absorption of photons having energy greater than its band gap. This excitation promotes an electron from the valence to the conduction band, which triggers a series of oxidation–reduction reactions involving the excited electron and the generated hole at the valence band [2]. Recently, solar-driven TiO_2 photocatalytic oxidation has attracted considerable attention in water treatment applications. It offers the possibility of using solar energy to activate the semiconductor. However, due to the TiO_2 wide band gap (3.2 eV) its photoactivity is limited to ultraviolet irradiation ($\lambda < 380$ nm) and thus less than 5% of the solar spectrum can be exploited [3]. In general, doping TiO_2 appears to be an effective way to overcome this limitation, since the photoactivity of the doped semiconductor may be extended to the visible-light region [4,5]. Boron doping constitute a way to accomplish it, since O atoms in the TiO_2 lattice can be substituted by B atoms mixing the p orbital of B with O 2p orbitals, narrowing the band gap and thus shifting the optical response into the visible range [5]. On the other hand, boron can also be located in interstitial positions of the TiO_2 lattice leading to the partial reduction of Ti(IV) to Ti(III), which could act as an electron trap enhancing the photocatalytic activity of TiO_2 [5,6].

Another way to improve the performance of TiO_2 photocatalytic systems is its simultaneous application with other AOPs, such as ozonation. The combined application of ozone and TiO_2 photocatalysis, known as photocatalytic ozonation, leads to a synergistic effect due to enhanced production of reactive oxygen species (ROS) such as hydroxyl radicals in comparison with the application of either single ozonation or single TiO_2 photocatalysis [7,8].

* Corresponding author. Tel.: +34 924289383; fax: +34 924289385.
E-mail address: anarey@unex.es (A. Rey).

http://dx.doi.org/10.1016/j.apcatb.2014.10.036
0926-3373/

In this study, the degradation of four herbicides and pesticides: diuron (DIU), o-phenylphenol (OPP), 2-methyl-4-chlorophenoxyacetic acid (MCPA) and terbuthylazine (TBA), commonly found in water ecosystems, has been studied. Their molecular structures can be found in Table S1 of the supplementary material. The degradation methods used were photocatalysis, ozonation, photolytic ozonation, and photocatalytic ozonation. Different boron doped TiO_2 photocatalysts (B-TiO_2) were synthesized and used in the photocatalytic treatments.

2. Experimental

2.1. Catalysts preparation

The synthesis of TiO_2 and B-TiO_2 catalysts was carried out following a sol–gel procedure previously reported [9]. Initially, a precursor solution was prepared by diluting the required amount of boric acid (Fisher Scientific) in 10 mL anhydrous ethanol (Panreac, 99.5%), then adding 4.26 mL tert-butyl titanate (Sigma–Aldrich, 97%), adjusting the pH to 3–4 with glacial acetic acid (Merck) and stirring for 30 min. After that, 20 mL ethanol were added to the precursor solution and the stirring was kept for two more hours. Ammonia aqueous solution (Fisher Scientific, 35%) was then added dropwise to reach pH 9. Afterward 10 mL ethanol was added and stirring was kept for another 30 min. The suspension was centrifuged and washed with ethanol three times. The resulting solid was dried at 60 °C overnight, manually grinded and finally calcined at 500 °C for 30 min. Catalysts with 3, 6, 9 and 12 wt.% of B were prepared. The nomenclature and some parameters of the catalysts are shown in Table 1. A fraction of catalysts with 6 and 12 wt.% of B were washed with ultrapure water to analyze the effect of B leaching.

2.2. Characterization of the catalysts

The characterization of the catalysts was carried out by inductively coupled plasma optical spectroscopy, N_2 adsorption–desorption, X-ray diffraction (XRD), X-ray photoelectron spectroscopy (XPS), and DR-UV-Vis spectroscopy.

Total B content of the catalysts was analyzed by inductively coupled plasma with an ICP-OES Optima 3300DV (Perkin–Elmer) after acidic microwave digestion of the samples.

BET surface area and pore structure of catalysts were determined from their nitrogen adsorption–desorption isotherms obtained at −196 °C using an Autosorb 1 apparatus (Quantachrome). Prior to analysis the samples were outgassed at 250 °C for 12 h under high vacuum (<10^{-4} Pa).

The crystalline structure was analyzed by X-ray diffraction (XRD) using a Bruker D8 Advance XRD diffractometer with a CuKα radiation (λ = 0.1541 nm). The data were collected from 2θ = 20° to 80° at a scan rate of 0.02 s^{-1} and 1s per point.

XPS spectra were obtained with a Kα Thermo Scientific apparatus with an AlKα ($h\nu$ = 1486.68 eV) X-ray source using a voltage of 12 kV under vacuum (2×10^{-7} mbar). Binding energies were calibrated relative to the C1s peak at 284.6 eV.

Diffuse reflectance UV-Vis spectroscopy (DR-UV-Vis) measurements, useful for the determination of the semiconductor band gap, were performed with an UV-Vis-NIR Cary 5000 spectrophotometer (Varian-Agilent Technologies) equipped with an integrating sphere device.

Transmitted photon flux through a catalyst suspension was analyzed by actinometrical measurements following the method proposed by Loddo et al. in [10], using the solar simulator described below with 250 mL of actinometrical solution and 250 mL of catalyst suspension at 0.33 g L^{-1}. Incident radiation flux was determined with ultrapure water replacing the catalyst suspension and was found to be 8.96×10^{-4} einstein min^{-1}.

2.3. Photocatalytic activity measurements

Photocatalytic experiments were carried out in a laboratory-scale system consisting of a 250 mL pyrex made 3-neck round-bottom flask (8.8 cm outer diameter) provided with a gas inlet, a gas outlet and a liquid sampling port. The reactor was placed in the chamber of a commercial solar simulator (Suntest CPS, Atlas) equipped with a 1500 W air-cooled Xe lamp with emission restricted to wavelengths over 300 nm (quartz and glass cut-off filters). The emission spectrum of the solar simulator can be seen in Fig. S1 of the supplementary material. The irradiation intensity was kept at 550 W m^{-2} and the temperature of the system was maintained between 25 and 40 °C throughout the experiments. If required, a laboratory ozone generator (Anseros Ozomat Com AD-02) was used to produce a gaseous ozone–oxygen stream that was fed to the reactor.

In a typical photocatalytic ozonation experiment, the reactor was first loaded with 250 mL of an aqueous solution containing 5 mg L^{-1} initial concentration of each pesticide (in a mixture). Then, the catalyst was added at a concentration of 0.33 g L^{-1} and the suspension was stirred in the darkness for 30 min (dark adsorption stage). Then, the lamp was switched on and, simultaneously, a mixture of ozone–oxygen (5 mg L^{-1} ozone concentration) was fed to the reactor at a flow rate of 10 L h^{-1}. The irradiation time for each experiment was 2 h. Samples were withdrawn from the reactor at intervals and filtered through a 0.2 μm PET membrane to remove the photocatalyst particles.

Photolysis experiments (i.e., absence of catalyst and ozone), adsorption (i.e., absence of radiation and ozone), ozonation alone (i.e., absence of radiation and catalyst), and photolytic ozonation (i.e., absence of catalyst) were also carried out for comparative purposes.

Pesticides concentrations were analyzed by HPLC (Hewlett Packard) provided with a Kromasil C18 column (5 μm, 150 mm long, 4 mm diameter, Teknokroma). As mobile phase a mixture of acetonitrile (solvent A) and 0.1% (v/v) phosphoric acid solution (solvent B) was used at 1 mL min^{-1}. Initially the mobile phase composition was varied from 40 to 25% solvent A in 12.5 min, then

Table 1
Nomenclature and some properties of the B-TiO_2 catalysts.

Catalyst	B (wt.%)	d_A (nm)	S_{BET} (m^2 g^{-1})	V_P (cm^3 g^{-1})	$(B/Ti)_{ICP}$ (at./at.)	$(B/Ti)_{XPS}$ (at./at.)	E_g (eV)
TiO_2	n.d.	16.8	68.3	0.102	0	0	3.07
3B-TiO_2	0.91	9.9	121.3	0.209	0.068	0.469	3.12
6B-TiO_2	1.06	9.2	120.1	0.147	0.079	0.531	3.03
9B-TiO_2	1.81	7.6	122.4	0.163	0.137	0.541	3.05
12B-TiO_2	3.55	7.5	125.5	0.180	0.273	0.693	3.01
6B-TiO_2-w	0.42	9.8	n.m.	n.m.	0.031	0.018	n.m.
12B-TiO_2-w	0.49	7.9	n.m.	n.m.	0.036	0.029	n.m.

n.d.: not detected, n.m.: not measured.

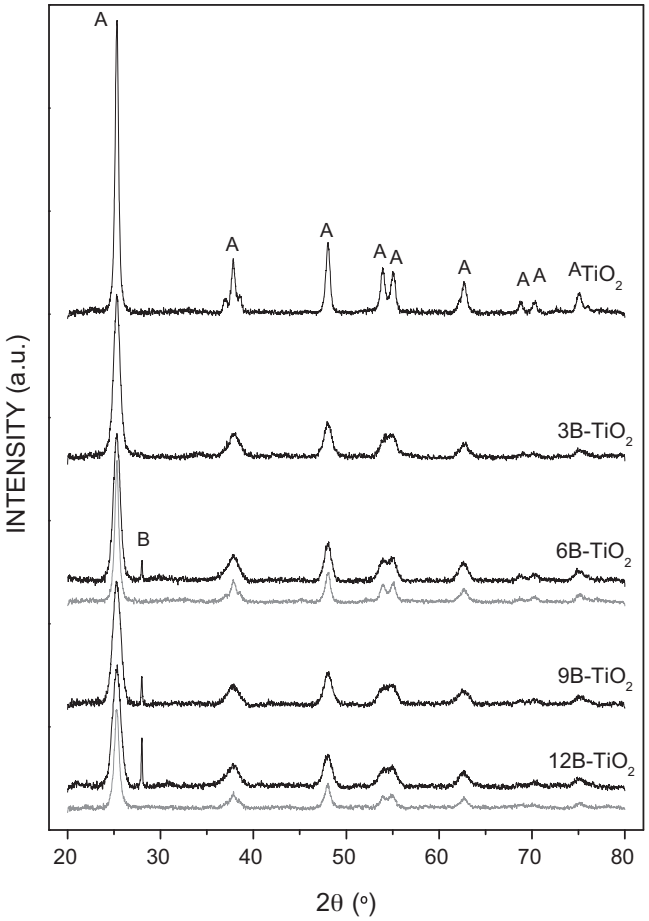

Fig. 1. XRD patterns of the photocatalysts (gray: washed samples, A: anatase, B: boron B_2O_3/H_3BO_3).

varied to 40% in 7.5 min and finally maintained at that composition for more 10 min. The retention times for DIU, MCPA, TBA and OPP were 10, 15.2, 23.2 and 25.8 min, respectively. The detection system was set at 220 nm.

Total organic carbon content (TOC) was measured using a Shimadzu TOC-V_{SCH} analyzer. Dissolved ozone was measured photometrically by following the indigo method at 600 nm [11]. Ozone in the gas phase was continuously monitored by means of an Anseros Ozomat GM-6000Pro analyzer. Hydrogen peroxide concentration was determined photometrically by the cobalt/bicarbonate method at 260 nm [12]. Boron leached from the catalysts was determined photometrically after complexation with azomethine-H at 410 nm [13]. Photometric measurements were carried out in a UV-Visible spectrophotometer (Evolution 201, Thermospectronic).

3. Results and discussion

3.1. Catalysts characterization

Table 1 summarizes some characteristics of the B-doped TiO_2 catalysts. Firstly, it can be noticed that the amounts of B incorporated to the catalysts are much lower than the theoretical values. Similar results have been observed in previous studies where around only 5–10% of the theoretical B was introduced in the final catalyst following sol–gel synthesis techniques [14,15].

The structure of the catalysts was analyzed by means of XRD and diffraction patterns are shown in Fig. 1. Anatase was identified as the only TiO_2 crystalline phase in all the catalysts together with the appearance of the sassolite boron structure (H_3BO_3) with the main diffraction peak at $2\theta = 28^\circ$ for the catalysts with B content equal or greater than the theoretical 6 wt.%. In addition, from the XRD patterns it can also be noticed that anatase diffraction peaks intensity decreased with the increasing B content. The crystallite size of anatase in the catalysts was calculated through Scherrer's equation. The values, which are shown in Table 1, reveal that the crystal size decreases with the increasing B content. This effect has been previously reported for similar catalysts and it has been attributed to the restrained TiO_2 crystal growing due to the existence of large amount of boron [16–18].

Textural parameters (BET surface area and total pore volume) were calculated from the adsorption–desorption isotherms presented in Fig. S2 of the supplementary information and are summarized in Table 1. In general, the sol–gel synthesis procedure together with the relatively short time of calcination led to catalysts with fairly high surface areas. In addition, it can be observed that both, BET surface area and total pore volume, increased with the increasing B content, effect that can be attributed to the lower crystal size of the anatase phase in the B-TiO_2 catalysts [16].

Surface composition of the TiO_2 and B-TiO_2 catalysts was analyzed by XPS. Fig. 2A shows, as an example, the high-resolution XPS spectra of the B 1s spectral region corresponding to 12B-TiO_2 catalyst. The binding energy for B 1s core level in H_3BO_3 or B_2O_3 is centered at 193.0 eV (B—O bond), whereas B located in the TiO_2 lattice corresponding to B occupying O sites as B—Ti bond in TiB_2 or O—Ti—B, and interstitial B as Ti—O—B presents lower binding energies at 187.5, 189.6 and 191.7 eV, respectively [16,18,19]. The symmetric peak found for all the B-TiO_2 catalysts was at 192.6 eV, thus indicating that B is mainly as H_3BO_3 or B_2O_3 in the catalysts surface, according to XRD results. However, the shift observed from 193.0 eV may be also indicative of the contribution of interstitial B. The presence of substitutional B (O—Ti—B or TiB_2) can be disregarded according to the absence of signal at binding energies lower than 190 eV. Ti 2p spectral region for 12B-TiO_2 and TiO_2 catalysts is depicted in Fig. 2B. The binding energy of the Ti 2p core levels at 464.5 and 458.7 eV, and the separation of the peaks around 5.8 eV, confirm the valence state of Ti(IV) in TiO_2 [20,21]. However, for 12B-TiO_2 catalysts the peaks have been shifted toward higher binding energy values that can be explained on the basis of the higher electronegativity of boron, thus confirming the formation of Ti—O—B structures (interstitial B) [16]. Finally, Fig. 2C shows the high-resolution XPS spectra of O 1s spectral region for TiO_2 and 12B-TiO_2 catalysts. The main peak located around 530 eV corresponds to Ti—O bonds with a widening at higher binding energy that has been assigned to hydroxyl groups in the TiO_2 surface. On the other hand, a second contribution to the O 1s spectra is observed in the boron doped catalyst at 532.4 eV corresponding to B—O bonds in H_3BO_3 or B_2O_3 [18]. Boron to titanium atomic surface ratio was calculated for all the catalysts from peak areas and Wagner atomic sensitivity factors [22]. These results are summarized in Table 1 together with B/Ti bulk ratio calculated from ICP results. It can be noticed that the surface ratios are larger than bulk ratios, suggesting that most of B is located on the surface of TiO_2 during the sol–gel synthesis. This has also been previously reported in La—B co-doped TiO_2 catalysts [14,23].

Table 1 also reports the band gap energy of the catalysts determined according to Tauc's expression from the UV–vis diffuse reflectance spectra (Figs. S3 and S4 of the supplementary material). The E_g value for bare TiO_2 was 3.07 eV, whereas for B-doped catalysts fluctuated from 3.01 to 3.12 eV with no distinguishable trend with the increasing B content. This is in a good agreement with previous results from Zaleska et al. [18] who reported similar values of E_g for B-doped TiO_2 catalysts with B content from 0.5 to 10 wt.%. This is likely the result of low or no mixing of 2p boron

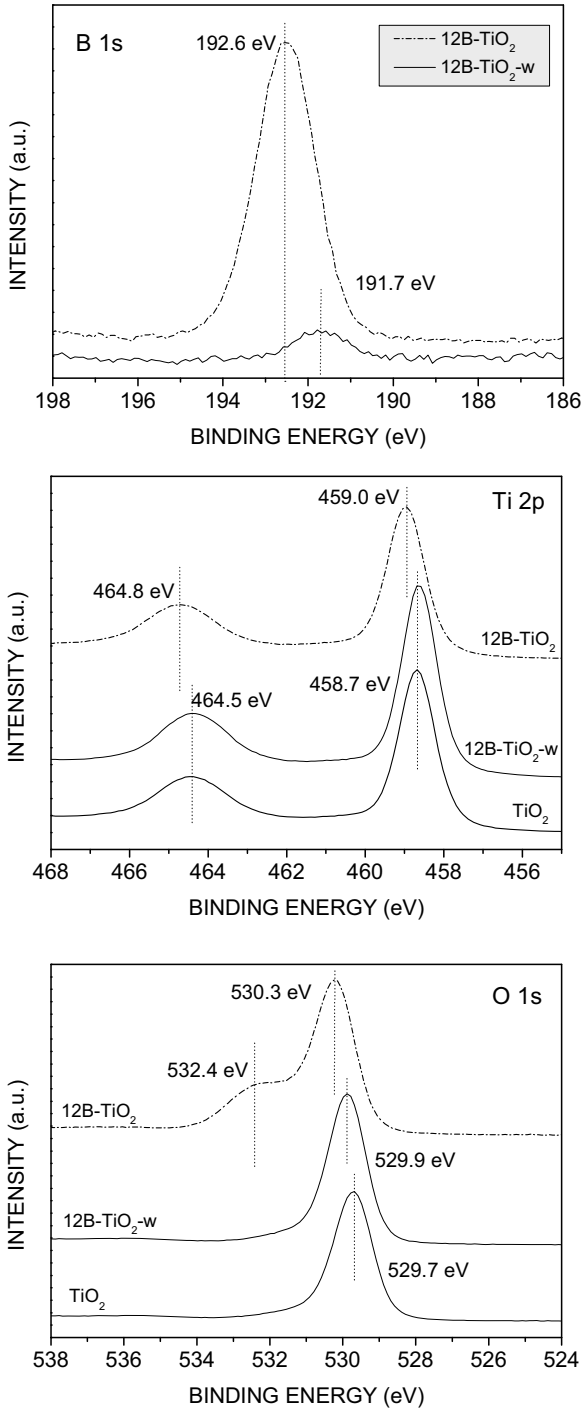

Fig. 2. High resolution XPS spectra of B 1s, O 1s and Ti 2p spectral regions of the catalysts TiO_2, 12B-TiO_2 and 12B-TiO_2-w.

bands with 2p oxygen bands since no substitutional B is achieved [5].

The catalysts were tested in photocatalysis and photocatalytic ozonation of the selected pesticides DIU, MCPA, TBA and OPP (not shown). However, during the experiments, dissolved boron was detected in the reaction medium, suggesting leaching to some extent. To analyze the leaching phenomenon, the catalysts were submitted to water washing at the same conditions of the reaction medium (catalyst concentration and pH). These results for 12B-TiO_2 photocatalyst are depicted in Fig. 3 together with the evolution of dissolved boron during the photocatalytic ozonation treatment. It

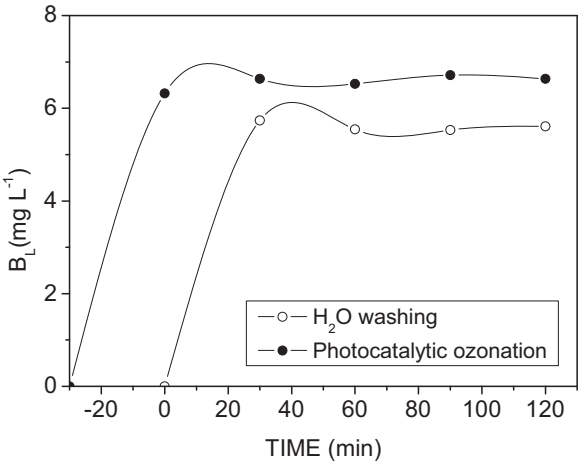

Fig. 3. B leaching of the 12B-TiO_2 catalyst during washing procedure and photocatalytic ozonation reaction (0.33 g L^{-1}).

can be noticed that unstable boron was leached from the catalyst surface to the aqueous solution just at the beginning of the test and then remained constant up to 2 h. The differences found between pesticides solution or water washing are lower than 1 mg L^{-1} of B and can be due to experimental deviations.

Total boron leached from all the catalysts during the washing procedure is summarized in Table 2. Boron concentration in solution reached values as high as 5.5 mg L^{-1} in the case of the highest loading B-doped catalyst, being the loss of the total boron from 46 to 70%. To our knowledge, boron leaching phenomenon has not been previously considered in B-doped TiO_2 catalysts application to wastewater treatment but it is mandatory since the limit of B ions in drinking water is 1 mg L^{-1} according to the European Union standards [24].

On the basis of these results, two of the catalysts were washed with ultrapure water until no dissolved boron was detected (6B-TiO_2-w and 12B-TiO_2-w catalysts). Some characterization results of the washed samples are summarized in Table 1. It can be observed a decrease of B bulk content until 0.42–0.49%. The similar percentage of boron after washing both catalysts suggests that only this amount can be introduced in the TiO_2 lattice regardless of the initial amount of boron used. XRD patterns of the washed catalysts do not display the diffraction peak of boron species H_3BO_3 or B_2O_3 but, as expected, the washing procedure did not substantially modify the crystal size of the anatase phase. In this line, it is reasonable to assume that no significant changes in the textural properties due to washing procedure develop. On the other hand, the washed catalysts were analyzed by XPS and the results of 12B-TiO_2-w are also plotted in Fig. 2 for comparative purposes. First of all, the intensity of the B 1s core level signal decreased significantly as a result of the loss of boron. However, the peak position located at 191.7 eV confirms the existence of boron in interstitial positions in the TiO_2 lattice (Ti—O—B bonds). The Ti 2p and O 1s spectra of 12B-TiO_2-w catalyst were similar to those of bare TiO_2. These results seem to point out that only a small portion of the initial boron was

Table 2
B leaching from the B-TiO_2 catalysts during washing procedure (0.33 g L^{-1}).

Catalyst	B (mg L^{-1})	B (%)
TiO_2	n.d.	n.d.
3B-TiO_2	1.83	60.6
6B-TiO_2	1.91	54.3
9B-TiO_2	4.20	69.9
12B-TiO_2	5.50	46.6

n.d.: not detected.

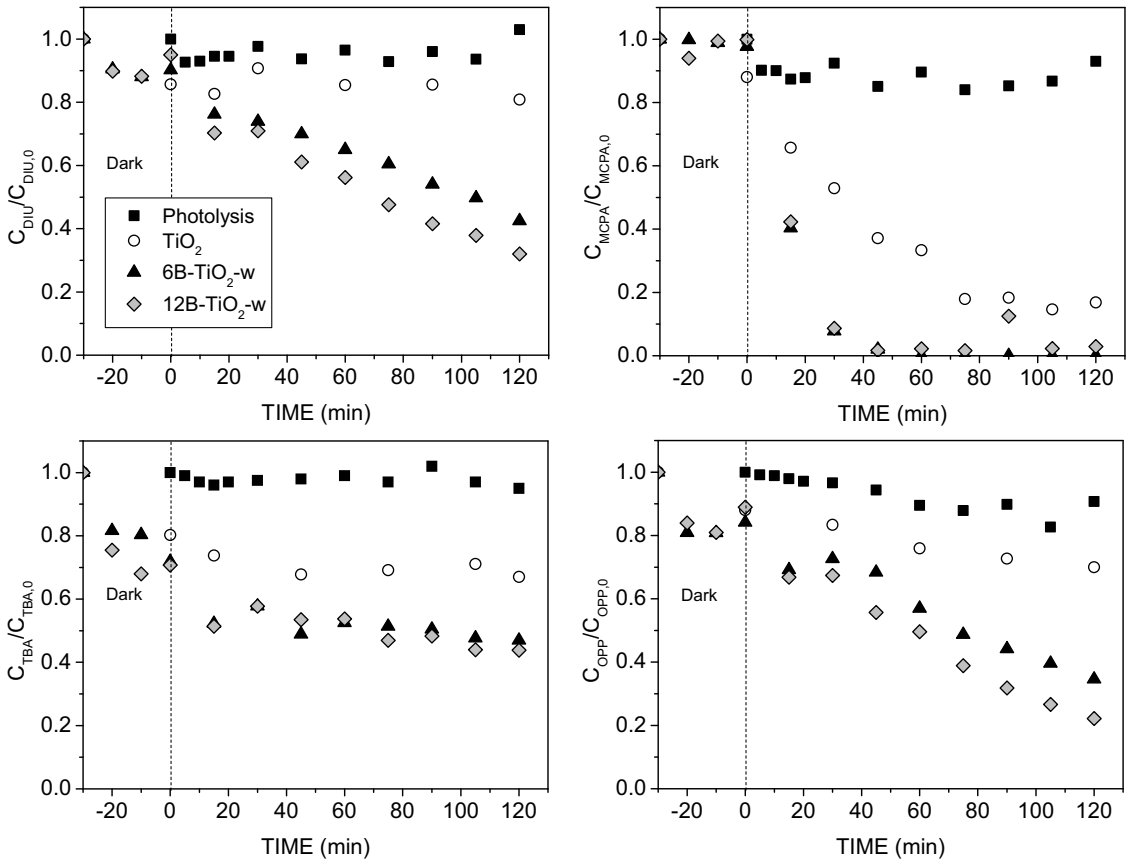

Fig. 4. Evolution of dimensionless herbicides and pesticides concentration during photocatalysis with TiO_2 and B-TiO_2 catalysts. Conditions: $pH_0 = 6.5$, $T = 25–40\,^{\circ}C$, $C_{PES,0} = 5\,mg\,L^{-1}$ (in the mixture), $C_{CAT} = 0.33\,g\,L^{-1}$, $Q_g = 10\,L\,h^{-1}$ (O_2).

introduced as interstitial boron in the TiO_2 lattice during the sol–gel method used, and also that this B is strongly bonded and stable in aqueous suspension whereas the surface boron forming H_3BO_3 or B_2O_3 entities is easily dissolved. Two extra catalysts were prepared increasing the calcination time from 30 min to 1 h and 3 h, but this operating variable did not improve the B stability leading to similar results (not shown). In addition, besides the band gap, other optical properties of the catalysts such absorption and scattering could be modified through B incorporation. The transmitted photon flux through a catalyst suspension could be an indirect measurement of these properties. In that case, the percentage of transmitted photon flux was 58.1% for TiO_2, 47.7% for 6B-TiO_2-w and 76.7% for 12B-TiO_2-w. According to this, 6B-TiO_2-w is expected to make a better use of radiation although no trend with other properties was observed and additional analyses would be necessary to reach stronger conclusions.

3.2. Photocatalytic activity

B-doped washed catalysts were tested in the photocatalytic oxidation and photocatalytic ozonation of the selected pesticides and compared with bare TiO_2 using simulated solar light as radiation source. The evolution of DIU, MCPA, TBA and OPP during photocatalytic oxidation treatment is depicted in Fig. 4. The catalysts were stirred with the solution of the pesticides in the dark for 30 min to reach the adsorption equilibrium. Low adsorption capacity was observed for DIU, MCPA and OPP whereas around 20% of TBA adsorption was achieved. In general, the adsorption capacity increased in the B-doped catalysts likely due to their more developed surface area and porosity. Direct photolysis of the pesticides did not produce significant degradation of DIU, MCPA and TBA, though a slight decrease of OPP concentration up to 10% was observed. These results are consistent with the UV–vis absorbance spectra of the target compounds shown in Fig. S5. For photocatalytic oxidation with bare and B-doped TiO_2 photocatalysts, in general, the presence of the catalyst improves the depletion rate of all the pesticides, which show different reactivity in the mixture. The order of the reactivity was found to be MCPA > OPP > DIU > TBA. The rate constants of the reaction between these compounds and the hydroxyl radical are $k_{MCPA\text{-}HO} = 4.5 \times 10^9$, $k_{OPP\text{-}HO} = 9.8 \times 10^9$, $k_{DIU\text{-}HO} = 7.1 \times 10^9$, $k_{TBA\text{-}HO} = 2.8 \times 10^9\,M^{-1}\,s^{-1}$ [25,26]. It is commonly assumed that in photocatalytic oxidation, the main degradation of organics takes place through hydroxyl radicals, especially when direct photolysis and/or adsorption have negligible contributions. The highest degradation rate of MCPA was not in agreement with the order of reactivity derived from the rate constant values. It could be possible that the hydroxyl radical reaction was not the only predominant degradation route for MCPA. In fact, some organic peroxy radicals formed as intermediates during MCPA photocatalytic oxidation are responsible of an autocatalytic behavior, as previously reported [27].

The incorporation of B to the catalysts lattice conferred an important effect in its catalytic activity. Thus, the degradation rate of all the pesticides was clearly enhanced in the presence of 6B-TiO_2-w and 12B-TiO_2-w catalysts. Similar behavior was observed for DIU and OPP, as 70–80% degradation was achieved with 12B-TiO_2-w catalyst vs. 20–30% obtained with bare TiO_2. For MCPA, around 45 min were necessary to reach almost complete removal whereas around 10% of MCPA still remained in solution with TiO_2 after 120 min of treatment. TBA depletion also improved with B-doped catalysts, reaching around 50% degradation compared to 35%

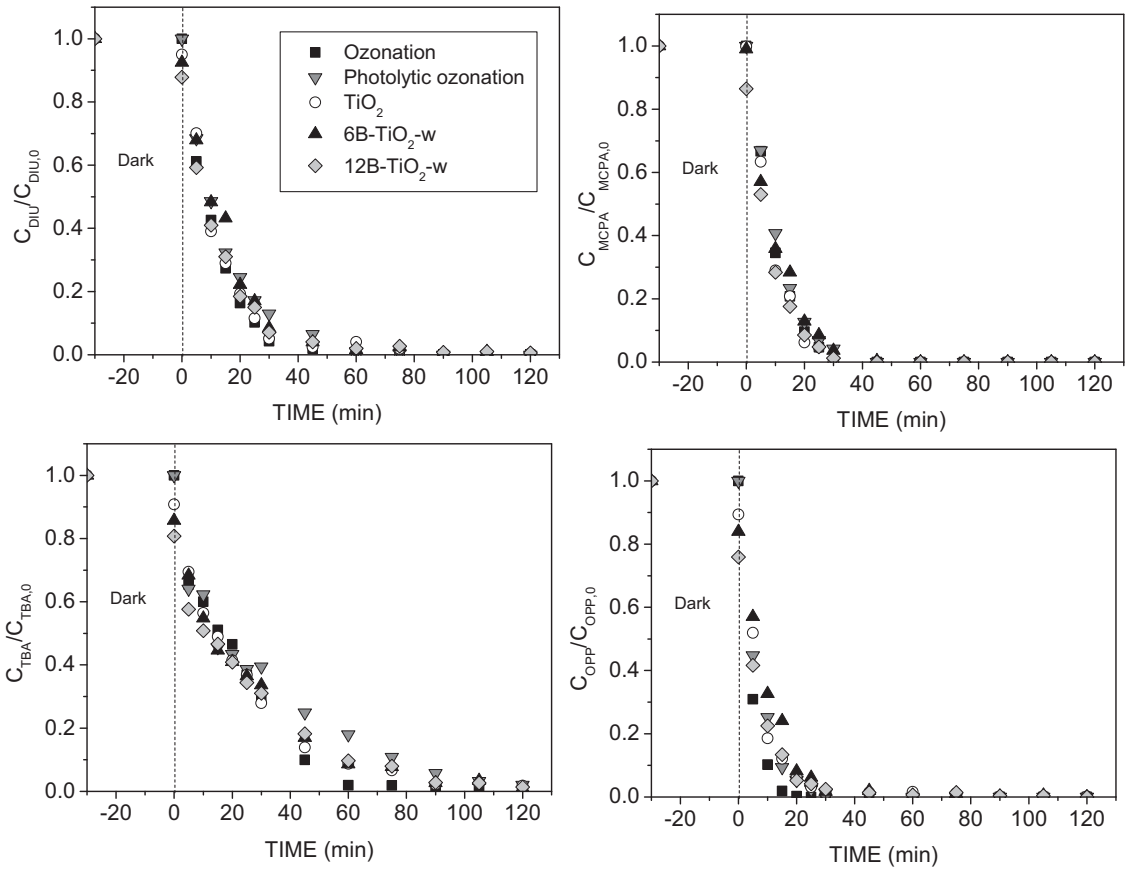

Fig. 5. Evolution of dimensionless pesticides concentration during ozone treatments with TiO_2 and B-TiO_2 catalysts. Conditions: $pH_0 = 6.5$, $T = 25–40\,^{\circ}C$, $C_{PES,0} = 5\,mg\,L^{-1}$ (in the mixture), $C_{CAT} = 0.33\,g\,L^{-1}$, $C_{O3ginlet} = 5\,mg\,L^{-1}$, $Q_g = 10\,L\,h^{-1}$ (O_3/O_2).

with TiO_2. However, TBA showed a refractory character toward its photocatalytic oxidation, since its concentration decreased faster during the first 15 min and then the degradation rate slowed down. These results point out the benefits of incorporating boron to the TiO_2 lattice. The role of B in interstitial positions of TiO_2 has not been unequivocally defined. It seems that B tends to lose its three valence electrons, which are donated to the 3d states of lattice Ti ions, thus giving rise to Ti(III) species. These latter have been postulated to reduce the recombination of photoexcited electrons and holes [5,28]. A boron content of about 0.5 wt.% seems to be enough to enhance the photocatalytic activity of TiO_2. The differences found in the activity of both doped catalysts could be related to the higher content of surface B detected by XPS in the 12B-TiO_2-w catalyst. On the other hand, the differences found in the textural properties and crystallinity of bare TiO_2 and B-TiO_2 catalysts might also play an important role in the behavior of the catalysts. However, it has been reported the improvement of photocatalytic performance with the increased crystallinity of the anatase particles since recombination process is prevented to some extent, though larger crystal size leads to lower specific surface areas [29]. Therefore, the improvement observed in the catalytic activity could be related to the presence of boron in TiO_2 interstitial positions more than to the changes produced in TiO_2 crystal size and textural properties. Also, the modification on the radiation absorption and scattering properties cannot be disregarded although transmitted photon flux measurements were not conclusive at this respect.

The evolution of the pesticides concentration during photocatalytic ozonation is shown in Fig. 5. Also, for comparative purposes, ozonation alone and the combination of ozone and radiation (photolytic ozonation) were applied. It can be observed that, regardless of the presence of catalysts and/or radiation, all the ozone treatments led to higher degradation rate of the pesticides than the photocatalytic oxidation process. The average time needed to reach 99% of pesticides removal with ozone treatments was around 60 min for DIU and TBA, and 30 min for MCPA and OPP. These are, in general, in agreement with the values of the rate constants of the ozone-pesticide reaction ($k_{MCPA\text{-}O3} = 323$, $k_{OPP\text{-}O3} = 379$, $k_{DIU\text{-}O3} = 3.7$, $k_{TBA\text{-}O3} = 20\,M^{-1}\,s^{-1}$ [25,30,31]). Nevertheless, indirect reactions due to ozone decomposition into hydroxyl radicals could take place at the reaction pH [32,33], also according with the high rate constant values between hydroxyl radical-pesticides commented above.

Main differences among the ozone treatments were found in terms of TOC removal. Previously, as seen in Fig. 6, in all cases, after the dark stage, low TOC removal due to adsorption on the catalysts was observed in comparison of the reaction stage. However, doped catalysts presented higher adsorption capacity compared to bare TiO_2, probably due to their higher surface areas. On the other hand, the TOC removal observed in the direct photolysis run was negligible, as expected. These results were improved by photocatalytic oxidation reaching 25% TOC removal with bare TiO_2 after 2 h. This mineralization level increased up to 37% and 45% using 6B-TiO_2-w and 12B-TiO_2-w catalysts, respectively. The higher efficiency of the doped catalysts compared to that of bare TiO_2 was also observed when applying the combined photocatalytic ozonation treatment. Although only 20% of the contaminant mixture was mineralized by single ozonation, the presence of radiation during photolytic ozonation increased up to 45% the mineralization degree. In the presence of radiation, a fraction of the ozone molecules that have not directly reacted with contaminants are

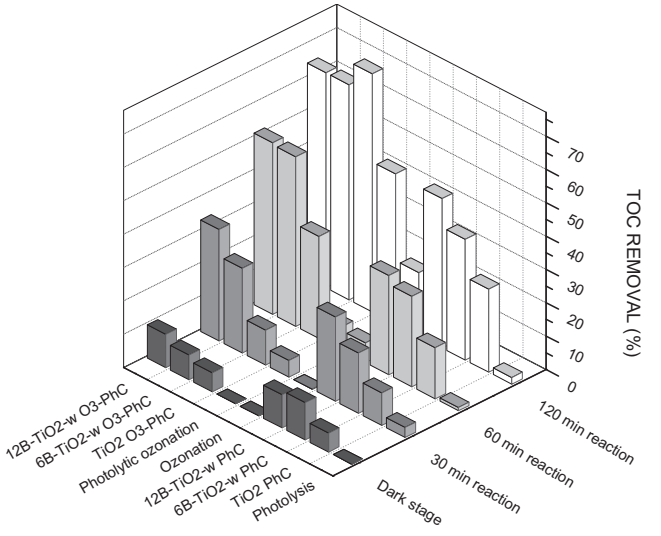

Fig. 6. TOC removal during all the treatments applied with TiO_2 and B-TiO_2 catalysts. Conditions: $pH_0 = 6.5$, $T = 25–40\ ^\circ C$, $C_{PES,0} = 5\ mg\ L^{-1}$ (in the mixture), $C_{CAT} = 0.33\ g\ L^{-1}$, $C_{O3ginlet} = 5\ mg\ L^{-1}$, $Q_g = 10\ L\ h^{-1}$ (O_3/O_2).

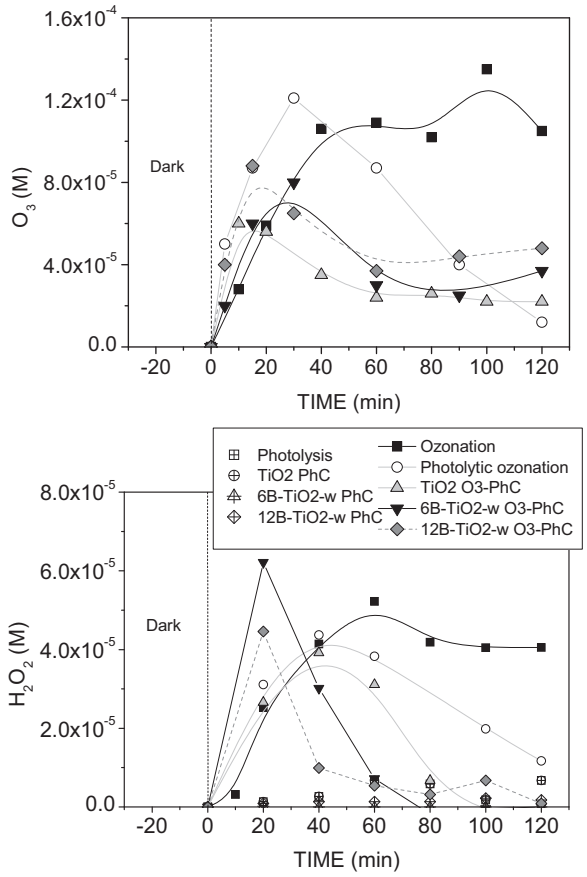

Fig. 7. Evolution of dissolved O_2 and H_2O_2 concentrations during all the treatments applied. Conditions: $pH_0 = 6.5$, $T = 25–40\ ^\circ C$, $C_{PES,0} = 5\ mg\ L^{-1}$, $C_{CAT} = 0.33\ g\ L^{-1}$, $C_{O3ginlet} = 5\ mg\ L^{-1}$ (in the mixture), $Q_g = 10\ L\ h^{-1}$ (O_3/O_2).

photolyzed under wavelengths near to 300 nm to produce reactive oxygen species (ROS), which enhance the mineralization rate [34]. These results were highly improved with the photocatalytic ozonation treatment, reaching 65–70% TOC removal. Ozone, as an electrophilic molecule, can trap electrons from the conduction band of the catalyst yielding ozonide ion radicals that decompose into ROS [7,8]. B-doped catalysts were more active than bare TiO_2 and led to faster mineralization rate according to TOC removal reached at 60 min reaction time, though the final mineralization degree was similar (around 1 mg L^{-1} TOC is the difference between bare and doped-TiO_2 catalysts at the end of the treatment).

It is known that hydrogen peroxide can be generated during photocatalytic treatments and also through direct ozone reactions [35–37]. The role of H_2O_2 and O_3 involved in photocatalytic reactions has been analyzed through the results depicted in Fig. 7. When comparing the dissolved ozone profiles (Fig. 7A) for single ozonation and photolytic ozonation it is observed that ozone accumulated in the solution from the beginning and its concentration remained almost constant along the experiment in contrast to photolytic ozonation which presented a maximum in the ozone concentration, which then decreased dramatically. This suggests that ozone is photolyzed with the radiation used to give rise to ROS, which enhanced the mineralization rate. The low accumulation of ozone in solution during the photocatalytic ozonation experiment can be explained taking into account the electrophilic character of ozone, which can act as an electron acceptor and trap the electrons photogenerated on the photocatalysts surface. On the other hand, the hydrogen peroxide concentration evolution is also shown in Fig. 7B. Photolysis and photocatalytic oxidation gave place to very low H_2O_2 concentrations. However, in all the ozone treatments the concentration of hydrogen peroxide was significantly higher. Thus, the formation of H_2O_2 through direct ozone reactions of the four pesticides was experimentally confirmed. During single ozonation, H_2O_2 concentration increased up to 40 min and then remained almost constant until the end of the experiment. A higher H_2O_2 decomposition rate was observed during photolytic ozonation, resulting in lower concentration at the end of the treatment. The H_2O_2 could undergo photolytic decomposition under wavelengths near 300 nm, thus improving the degradation and mineralization of the contaminants [38]. On the other hand, during photocatalytic ozonation with bare TiO_2 a higher decomposition rate of H_2O_2 was also observed, the concentration being negligible after 100 min of treatment. With B-doped TiO_2 catalysts, the formation of hydrogen peroxide took place at higher rate reaching a maximum concentration at about 20 min and then the consumption was also faster and the concentration negligible at the end of the treatment. These results point out that H_2O_2 is likely being consumed through photocatalytic reactions acting as electron acceptor in the TiO_2 surface. This process is more efficient with B-doped TiO_2 catalysts compared to bare TiO_2 also indicating their higher photocatalytic activity.

3.3. Catalyst stability

The stability and reusability of the 12B-TiO_2-w catalyst was tested in three consecutive runs of photocatalytic ozonation process. The catalyst was easily separated by sedimentation after each run and used without any treatment in the next experiment. After removing the supernatant solution, a new fresh solution of the four pesticides was added to start the following run. In all the experiments the catalyst from the previous run was kept 30 min in the darkness with the new fresh solution to reach adsorption equilibrium.

Taking into account that main differences found between the ozone treatments were found in mineralization, Fig. 8 shows TOC removal percentages during the dark adsorption stage and after 1 and 2 h of photocatalytic ozonation. During the dark stage, only slight changes were observed in adsorption capacity of the reused catalyst varying the percentage of TOC adsorbed between 3 and 7% with no trend which indicates that the small amount of initial pesticides adsorbed onto the catalyst surface is oxidized during the photocatalytic treatment. On the other hand, the mineralization reached at 2 h reaction time was maintained at about 75%

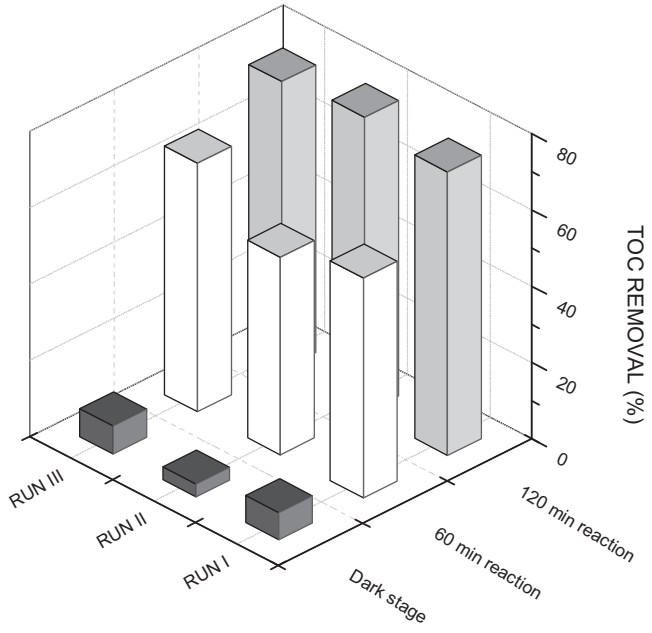

Fig. 8. TOC removal during consecutive photocatalytic ozonation runs. Conditions: $pH_0 = 6.5$, $T = 25–40\,^{\circ}C$, $C_{PES,0} = 5\,mg\,L^{-1}$ (in the mixture), $C_{CAT} = 0.33\,g\,L^{-1}$, $C_{O3ginlet} = 5\,mg\,L^{-1}$, $Q_g = 10\,L\,h^{-1}$ (O_3/O_2).

during the consecutive runs. Furthermore, the mineralization rate seems to slightly increase when compared TOC removal at 1 h reaction time being mineralization increased from 55 to 65% during the reutilization of the catalyst. In addition no boron leached was detected after the consecutive use of the catalyst. Therefore, although additional experiments would be needed to test the long term performance of the catalyst, this results point out the stability and reusability of these B-doped TiO_2 catalysts once the non-structural remaining boron was washed.

4. Conclusions

The sol–gel method used to dope the TiO_2 catalysts led to the incorporation of a lower amount of boron than the theoretical value. A part of the amount of boron on the catalysts was in the form of B_2O_3/H_3BO_3 species, which was unstable in aqueous solution and released boron to the reaction medium. An extra washing of the catalysts with water led to the removal of unstable boron and no further leaching. The rest of the boron on the catalysts was incorporated in interstitial positions of TiO_2 and did not modify the band gap energy with respect to bare TiO_2. The presence of boron on the catalysts also caused the reduction of the crystal size of the anatase particles of TiO_2 and an increase of the pore volume and specific surface area respect to the bare TiO_2. The washed B-doped TiO_2 were more active than bare TiO_2 for the removal and mineralization of the target compounds due to the effect of boron in interstitial positions of TiO_2 avoiding the recombination process to some extent. The efficiency of the studied systems regarding mineralization rate followed the order: single ozonation < photocatalysis with TiO_2 < photocatalysis with B-TiO_2 < photolytic ozonation < photocatalytic ozonation with TiO_2 < photocatalytic ozonation with B-TiO_2. Photocatalytic ozonation with B-TiO_2 catalysts was the most efficient process in terms of mineralization, leading to the complete removal of the pesticides in less than 90 min with 75% mineralization after 120 min. The catalytic activity was maintained after 3 consecutive runs with no leaching boron detected.

Acknowledgements

This work has been supported by the Spanish Ministerio de Economía y Competitividad (MINECO) and European Feder Funds through the project CTQ2012-35789-C02-01. Authors acknowledge the SAIUEX service of the University of Extremadura for the characterization analyses. D.H. Quiñones thanks the MINECO the concession of a predoctoral FPI grant and an aid for a research stay at the Loughborough University.

Appendix A. Supplementary data

Supplementary data associated with this article can be found, in the online version, at http://dx.doi.org/10.1016/j.apcatb.2014.10.036.

References

[1] A. Calzadilla, K. Rehdanz, R. Tol, J. Hydrol. 384 (2010) 292–305.
[2] A. Fujishima, T.N. Rao, D.A. Tryk, J. Photochem. Photobiol. C: Photochem. Rev. 1 (2000) 1–21.
[3] X. Gao, P. Chen, J. Liu, Mater. Lett. 65 (2011) 685–687.
[4] P. Dharmarajan, A. Sabastiyan, M. Yosuva Suvaikin, S. Titus, C. Muthukumar, Chem. Sci. Trans. 2 (2013) 1450–1458.
[5] M.V. Dozzi, E. Selli, J. Photochem. Photobiol. C: Photochem. Rev. 14 (2013) 13–28.
[6] N.S. Begum, H.M.F. Ahmed, O.M. Hussain, Bull. Mater. Sci. 31 (2008) 741–745.
[7] E.M. Rodríguez, G. Márquez, E.A. León, P.M. Álvarez, A.M. Amat, F.J. Beltrán, J. Environ. Manage. 127 (2013) 114–124.
[8] T.E. Agustina, H.M. Ang, V.K. Vareek, J. Photochem. Photobiol. C: Photochem. Rev. 6 (2005) 264–273.
[9] Z. Li, B. Gao, G.Z. Chen, R. Mokaya, S. Sotiropoulos, G. Li Puma, Appl. Catal. B: Environ. 110 (2011) 50–57.
[10] V. Loddo, M. Addamo, V. Augugliaro, L. Palmisano, M. Schiavello, E. Garrone, AIChE J. 52 (2006) 2565–2574.
[11] H. Bader, J. Hoigné, Water Res. 15 (1981) 449–456.
[12] W. Masschelein, M. Denis, R. Ledent, Spectrophotometric determination of residual hydrogen peroxide, in: Water Management. Water Sewage Works, 1977, August, pp. 69–72.
[13] F.J. López, E. Giménez, F. Hernández, Fresenius J. Anal. Chem. 346 (1993) 984.
[14] J.W. Liu, R. Han, H.T. Wang, Y. Zhao, W.J. Lu, H.Y. Wu, T.F. Yu, Y.X. Zhang, J. Mol. Catal. A: Chem. 344 (2011) 145–152.
[15] S. Bagwasi, B. Tian, J. Zhang, M. Nasir, Chem. Eng. J. 217 (2013) 108–118.
[16] W. Zhang, T. Hu, B. Yang, P. Sun, H. He, J. Adv. Oxid. Technol. 16 (2013) 261–267.
[17] D. Chen, D. Yang, Q. Wang, Z. Jiang, Ind. Eng. Chem. Res. 45 (2006) 4110–4116.
[18] A. Zaleska, J.W. Sobczak, E. Grabowska, J. Hupka, Appl. Catal. B: Environ. 78 (2008) 92–100.
[19] E. Finazzi, C. Di Valentin, G. Pacchioni, J. Phys. Chem. C 113 (2009) 220–228.
[20] M.W. Xiao, L. Wang, X.J. Huang, Y.D. Wu, Z. Dang, J. Alloys Compd. 470 (2009) 486–491.
[21] Y. Li, L. Chen, Y. Guo, X. Sun, Y. Wei, Chem. Eng. J. 181–182 (2012) 734–739.
[22] C.D. Wagner, L.E. Davis, M.V. Zeller, J.A. Taylor, R.H. Raymond, L.H. Gale, Surf. Interface Anal. 3 (1981) 211–225.
[23] X. Lan, L. Wang, B. Zhang, B. Tian, J. Zhang, Catal. Today 224 (2014) 163–170.
[24] Council of the European Union, Council Directive 98/83/EC of 3 November 1998. On the quality of water intended for human consumption, 1998.
[25] M. Olak-Kucharczyk, J.S. Miller, S. Ledakowicz, Ozonation kinetics of o-phenylphenol in aqueous solutions, Ozone Sci. Eng. 34 (2012) 300–305.
[26] B.A. Wols, C.H.M. Hofman-Caris, Water Res. 46 (2012) 2815–2827.
[27] J. Rivas, R.R. Solis, O. Gimeno, J. Sagasti, Int. J. Environ. Sci. Technol. (December) (2013), http://dx.doi.org/10.1007/s13762-013-0452-4.
[28] V. Gombac, L. De Rogatis, A. Gasparotto, G. Vicario, T. Montini, D. Barreca, G. Calducci, P. Fornasiero, E. Tondello, M. Graziani, Chem. Phys. 339 (2007) 111.
[29] M.A. Henderson, Surf. Sci. Rep. 66 (2011) 185–297.
[30] J.Y. Hu, T. Morita, Y. Magara, T. Aizawa, Water Res. 34 (2000) 2215–2222.
[31] F.J. Benítez, F.J. Real, J.L. Acero, C. García, Water Res. 41 (2007) 4073–4084.
[32] U. von Gunten, Water Res. 37 (2003) 1443–1467.
[33] F.J. Beltran, Ozone Reaction Kinetics for Water and Wastewater Systems, CRC Press, Boca Raton, FL, USA, 2004.
[34] L. Sánchez, X. Domenech, J. Casado, J. Peral, Chemosphere 50 (2003) 1085–1093.
[35] M. Mvula, C. von Sonntag, Org. Biomol. Chem. 1 (2003) 1749–1756.
[36] A. Leitzke, C. von Sonntag, Ozone Sci. Eng. 31 (2009) 301–308.
[37] S. Rakowski, D. Cherneva, Int. J. Chem. Kinet. 22 (1990) 321–329.
[38] J.H. Baxendale, J.A. Wilson, Trans. Faraday Soc. 53 (1957) 344–356.